Letter

High-temperature superconductivity in Li_2AuH_6 mediated by strong electron-phonon coupling under ambient pressure

Zhenfeng Ouyang,[1,2,*] Bo-Wen Yao,[1,2,*] Xiao-Qi Han,[1,2,*] Peng-Jie Guo,[1,2] Ze-Feng Gao,[1,2,†] and Zhong-Yi Lu[1,2,3,‡]

[1]*School of Physics and Beijing Key Laboratory of Opto-electronic Functional Materials & Micro-nano Devices, Renmin University of China, Beijing 100872, China*

[2]*Key Laboratory of Quantum State Construction and Manipulation (Ministry of Education), Renmin University of China, Beijing 100872, China*

[3]*Hefei National Laboratory, Hefei 230088, China*

(Received 22 January 2025; revised 6 March 2025; accepted 20 March 2025; published 2 April 2025)

We use our developed AI search engine (InvDesFlow) to perform extensive investigations regarding ambient stable superconducting hydrides. A cubic structure Li_2AuH_6 with Au-H octahedral motifs is identified to be a candidate. After performing thermodynamical analysis, we provide a feasible route to experimentally synthesize this material via the known LiAu and LiH compounds under ambient pressure. The further first-principles calculations suggest that Li_2AuH_6 shows a high superconducting transition temperature (T_c) $\sim$ 140 K under ambient pressure. The H-1*s* electrons strongly couple with phonon modes of vibrations of Au-H octahedrons as well as vibrations of Li atoms, where the latter is not taken seriously in other previously similar cases. Hence, different from previous claims of searching metallic covalent bonds to find high-T_c superconductors, we emphasize here the importance of those phonon modes with strong electron-phonon coupling (EPC). And we suggest that one can intercalate atoms into binary or ternary hydrides to introduce more potential phonon modes with strong EPC, which is an effective approach to find high-T_c superconductors within multicomponent compounds.

DOI: 10.1103/PhysRevB.111.L140501

Introduction. Searching superconducting materials with high transition temperature (T_c) is a hot issue since the discovery of superconductivity [1]. As the lightest element, high-T_c superconductivity was anticipated to realize in metallic hydrogen [2]. However, solid hydrogen is too difficult to stabilize and shows superconductivity under ambient pressure. Consequently, researchers are shifting their focus toward hydrogen-rich compounds under high-pressure conditions. In 2014, H_3S was theoretically predicted to exhibit superconductivity under high pressure [3,4], which was experimentally confirmed [5]. With the development of this high-pressure technique, various hydrogen-rich superconductors with high-T_c were synthesized, for example, LaH_{10} [6,7], YH_9 [8,9], and CaH_6 [10], which made the high-pressure hydride become a very promising candidate for room-temperature superconductivity.

However, extremely high pressure brings challenges to experimental synthesis as well as the characterization of the sample. Applying chemical pressure by introducing heavy atoms is an effective approach, which may decrease the required pressure. Based on this, many binary rare-earth hydrides ReH_n (Re = Ce, Pr, Nd, Eu, and Th) were theoretically proposed and successively synthesized [9,11–17], but most of them still required pressure of ~100 GPa.

In recent years, ternary hydride has received more attention due to the enlarged phase space and enhanced flexibility of its manipulation. Some superconducting ternary hydrides were theoretically proposed, for example, H_6SX (X = Cl, Br) [18], $LaRH_8$ (R = B, Be) [19–21], Li_2MgH_{16} [22], KB_2H_8 [23], and $CsBH_5$ [24]. Among them, the strong electron-phonon coupling (EPC) driven by the metallic B-H σ-bond and the related phonon in KB_2H_8 lead to a superconducting transition with T_c $\sim$ 134 K under 12 GPa. Furthermore, using chemical doping to modulate the virtual high-pressure effect, $CsBH_5$ exhibits superconductivity with T_c $\sim$ 98 K under near-ambient 1-GPa pressure. In addition, the ternary hydrides $LaBeH_8$ [25] (T_c $\sim$ 110 K under 80 GPa), LaB_2H_8 [26] (T_c $\sim$ 106 K under 90 GPa), and La-Ce-H system [27] (T_c $\sim$ 176 K under 100 GPa) were experimentally reported. These theoretical and experimental works suggested that ternary hydride was expected to exhibit high-T_c superconductivity under relatively low, even ambient pressure.

Very recently, Dolui *et al.*, performed an *ab initio* random structure search at 1 GPa and predicted various potential superconducting ternary hydrides $A_aB_bH_c$ [28]. A metastable cubic Mg_2IrH_6 with predicted transition T_c $\sim$ 160 K was revealed, which may be synthesized via a high-pressure route from insulating Mg_2IrH_7. Another group performed a machine-learning accelerated high-throughput investigation regarding Mg_2XH_6 (X = Rh, Ir, Pd, and Pt) compounds under ambient pressure, which suggested that superconducting T_c was in range of 45 to 80 K and the T_c of the Pt compound may be enhanced above 100 K via doping electrons [29].

*These authors contributed equally to this work.
†Contact author: zfgao@ruc.edu.cn
‡Contact author: zlu@ruc.edu.cn

High-throughput screening calculations of EPC in X_2MH_6 (X = Li, Na, Mg, Al, K, Ca, Ga, Rb, Sr, and In; M are transition metals) further predicted more compounds with superconducting T_c exceeding 50 K under ambient pressure, which enlarged this superconducting ternary 216-type family [30].

Techniques from machine learning and data science are increasingly being employed to address problems in materials science [31]. In particular, generative modeling methods based on autoencoder architectures and diffusion [32,33] have been employed to generate crystal structures. In this Letter, we perform vast investigations regarding ternary hydrides through our developed AI search engine, namely, InvDesFlow [32], which integrates generative AI and several graph neural networks for the discovery of high-T_c superconductors. See Supplemental Material [34] for the details of the mentioned AI search engine (see also Refs. [2,9] therein). The specific setting of the AI model can be found in the source code [35]. A high-T_c superconductor Li_2AuH_6 that is isostructural to Mg_2IrH_6 is identified. Combined with the first-principles density-functional theory and superconducting EPC calculations, Li_2AuH_6 shows a high-T_c $\sim$ 140 K under ambient pressure. Thermodynamic study suggests that Li_2AuH_6 is a metastable phase and may be experimentally synthesized via the known LiH and LiAu compounds. Detailed EPC analysis indicates that the H-1s electrons couple with special phonon modes and then drive strong Cooper pairing. Different from previous reports that emphasized the vibrations of H octahedrons, we find that the vibrations of Li atoms also contribute strong EPC, even stronger than that of the vibrations of H octahedrons. Our work reveals a ternary hydride Li_2AuH_6 with superconducting T_c $\sim$ 140 K under ambient pressure and suggests that EPC can be enhanced by introducing more strong coupling modes.

Methods. In this Letter, the density functional theory (DFT) calculations are performed by the first-principles package QUANTUM ESPRESSO [36]. The generalized gradient approximation of the Perdew-Burke-Ernzerhof formula [37] for the exchange and correlation functional is chosen. The optimized norm-conserving Vanderbilt pseudopotential is used [38]. The kinetic energy cutoff and the charge density cutoff are respectively set to be 80 Ry and 320 Ry. The charge densities are self-consistently calculated on an unshifted 16 × 16 × 16 **k**-point mesh grid with a Methfessel-Paxton smearing of 0.02 Ry [39]. In addition, the phonons are calculated on a 4 × 4 × 4 **q**-point mesh grid based on the density-functional perturbation theory [40].

The Wannier interpolation technique is used to calculate electron-phonon coupling superconductivity with electron-phonon Wannier (EPW) codes [41]. The maximally localized Wannier functions (MLWFs) [42] are constructed on a 4 × 4 × 4 **k**-point mesh grid. The Au-5d, and H-1s orbitals are projected. The convergent EPC constant λ is extensively carried out through fine electron (48 × 48 × 48) and phonon (16 × 16 × 16) grids and the dirac δ functions for electrons and phonons awere smeared out by a Gaussian function with widths of 90 meV and 0.5 meV, respectively. The anisotropic Eliashberg equations [41,43,44] are solved on a fine electron grid of 48 × 48 × 48 points. The sum over Matsubara

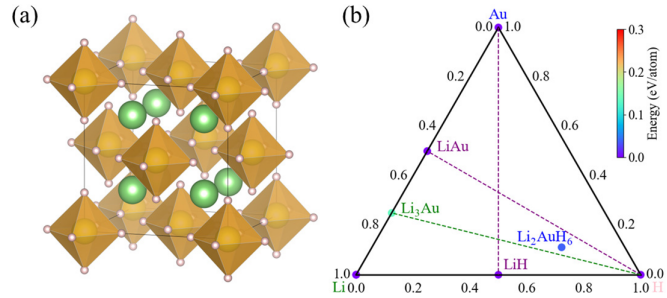

FIG. 1. (a) Crystal structure of Li_2AuH_6. The green, yellow, and pink balls denote the Li, Au, and H atoms, respectively. The Au-H octahedrons are presented by golden surfaces. (b) Ternary convex hulls of Li-Au-H systems.

frequencies is truncated with $\omega_c = 1.7$ eV, about ten times that of the highest phonon frequency.

According to the Migdal-Eliahsberg theory [45], the mode- and wave-vector-dependent coupling $\lambda_{\mathbf{q}\nu}$ reads

$$\lambda_{\mathbf{q}\nu} = \frac{2}{\hbar N(0) N_{\mathbf{k}}} \sum_{nm\mathbf{k}} \frac{1}{\omega_{\mathbf{q}\nu}} \left| g^{nm}_{\mathbf{k},\mathbf{q}\nu} \right|^2 \delta\left(\epsilon^n_{\mathbf{k}}\right) \delta\left(\epsilon^m_{\mathbf{k}+\mathbf{q}}\right), \tag{1}$$

where $N(0)$ is the density of states (DOS) of electrons at the Fermi level. $N_{\mathbf{k}}$ is the total number of **k** points in the fine **k**-mesh. $\omega_{\mathbf{q}\nu}$ is the phonon frequency and $g^{nm}_{\mathbf{k},\mathbf{q}\nu}$ is the EPC matrix element. (n, m) and ν denote the indices of bands and the phonon mode, respectively. $\epsilon^n_{\mathbf{k}}$ and $\epsilon^m_{\mathbf{k}+\mathbf{q}}$ are the band eigenvalues with respect to the Fermi level. By the summation of $\lambda_{\mathbf{q}\nu}$ over the first Brillouin zone, or the intergration of the Eliahberg spectral function $\alpha^2F(\omega)$, the EPC constant λ is determined

$$\lambda = \frac{1}{N_{\mathbf{q}}} \sum_{\mathbf{q}\nu} \lambda_{\mathbf{q}\nu} = 2 \int \frac{\alpha^2 F(\omega)}{\omega} d\omega, \tag{2}$$

where $N_{\mathbf{q}}$ represents the total number of **q** points in the fine **q**-mesh. The Eliashberg spectral function $\alpha^2F(\omega)$ is calculated by

$$\alpha^2 F(\omega) = \frac{1}{2N_{\mathbf{q}}} \sum_{\mathbf{q}\nu} \lambda_{\mathbf{q}\nu} \omega_{\mathbf{q}\nu} \delta(\omega - \omega_{\mathbf{q}\nu}). \tag{3}$$

Results and Analysis. Figure 1(a) shows the crystal structure of Li_2AuH_6. Li atoms are intercalated into the interstitial position between Au-H octahedrons and occupy the Wyckoff sites 8c (0.25, 0.25, 0.25). Many similar 216-type structures were theoretically proposed in previous works while a considerable number of them are energetically unfavorable under ambient pressure, which implied a difficulty for experimental synthesis. Hence, we first focus the thermodynamic property of Li_2AuH_6. As shown in Fig. 1(b), there are two possible approaches that may synthesize Li_2AuH_6 from the Li-Au alloy. Our calculations suggest that LiAu possesses a lower formation energy ~ -0.54 eV/atom at ambient pressure than Li_3Au (−0.41 eV/atom), which is consistent to a previous report [46]. The formation energy is defined as

$$\Delta E(\mathrm{Li}_m\mathrm{Au}_n) = \frac{E(\mathrm{Li}_m\mathrm{Au}_n) - mE(\mathrm{Li}) - nE(\mathrm{Au})}{m+n}. \tag{4}$$

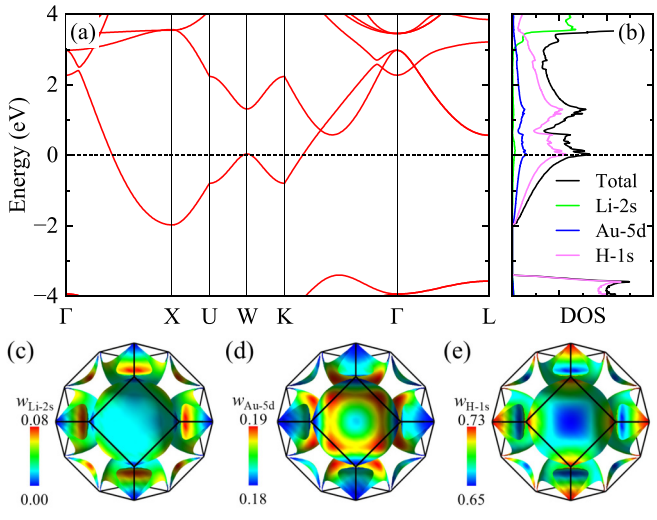

FIG. 2. Electronic structure of Li_2AuH_6 for (a) band structure and (b) atomic orbital-projected density of states (PDOS). The Fermi level is set to zero. (c)–(e) The Fermi surfaces with orbital weight of the Li-2*s*, Au-5*d*, and H-1*s* orbitals, respectively.

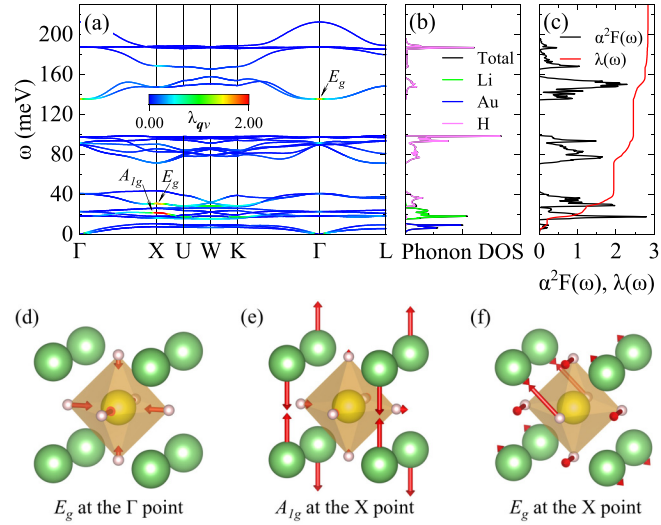

FIG. 3. (a) Phonon spectrum with a color representation of $\lambda_{\mathbf{q}\nu}$ under ambient pressure. (b) Total and projected phonon DOS. (c) Eliashberg spectral function $\alpha^2F(\omega)$ and accumulated $\lambda(\omega)$. The graduation of $\alpha^2F(\omega)$ is omitted for clarify. (d)–(f) The vibration modes for E_g at the Γ point, A_{1g} at the *X* point, and E_g at the *X* point, respectively.

Hence, we propose a feasible route $6LiH + 5Au \rightarrow Li_2AuH_6 + 4LiAu$. The calculated formation energy of the right side of the equation is only ∼38meV/atom higher than that of the left side. As for such a solid metastable phase, the reaction kinetics under ambient condition may be slow, hence catalysts may be used. In addition, the metastable structure may decompose or transform into other phases during synthesis, which suggests that rapid quenching, inert gas atmospheres, or encapsulation may be needed. In a word, according to a survey [47], the lower formation energy than a typical value of 80 meV/atom implies a good experimental synthesizability. These results suggest that Li_2AuH_6 is a metastable phase that may be experimentally synthesized.

Figure 2(a) shows that Li_2AuH_6 is a metal with one band crossing the Fermi level. In addition, the calculated projected density of states (PDOS) in Fig. 2(b) suggests that electrons from Au-H octahedrons contribute almost all the electronic states around the Fermi level. A van Hove singularity is found at the *W* point, which contributes a high peak of PDOS at the Fermi level. In Figs. 2(c)–2(e), we show the Fermi surfaces with orbital weight. The contribution of the Li-2*s* orbital is negligible due to the weak electronegativity of Li. The relatively low fraction of Au-5*d* orbitals leads to an anisotropic distribution of electronic states upon the Fermi surfaces. For example, in the hemispherical Fermi surfaces, the H-1*s* orbital possesses significantly different weights around the *W* point and at the bottom of hemisphere.

Next, we investigate the phonon and EPC of Li_2AuH_6 under ambient pressure. As shown in Fig. 3(a), no trace of the imaginary phonon mode is found under the ambient pressure, which suggests that Li_2AuH_6 is dynamically stable. We also study some other similar structures where the Au atom is respectively replaced by Pd, Ag, and Pt. We find that the Au-H octahedron shows unique stability under ambient pressure, while the same case of Pd and Ag show a maximum imaginary phonon ~ -3.2 and -19 meV, respectively, and Li_2PtH_6 is a band insulator. As shown in Fig. 3(b), the phonon spectrum of Li_2AuH_6 can be divided into three regions, and two obvious energy gaps are observed. Specifically, the high-frequency region above 120 meV and the medium-frequency region ranging from 60 to 100 meV are totally contributed to by vibrations of H atoms. Acoustic phonons and relatively low-frequency optical branches below 50 meV are respectively contributed to by the vibrations of Au and Li mixed with H.

Furthermore, our EPC calculations suggest that the EPC constant λ of Li_2AuH_6 is 2.84, and there are three phonon modes that contribute strong EPC; they are the E_g mode ∼140 meV at the Γ point, the A_{1g} mode ∼20 meV at the *X* point, and the E_g mode ∼30 meV at the *X* point, which are labeled in Fig. 3(a). As shown in Fig. 3(d), the E_g mode at the Γ point is a breathing mode of the Au-H octahedron. This vibration mode may cause strong changes of distribution of charge density, hence providing a strong EPC. This has been mentioned in the studies of other 216-type structures containing H octahedrons. However, the A_{1g} and E_g modes at the *X* point are also identified as inducing strong EPC in Li_2AuH_6. These two modes contain vibrations of Li atoms besides those of the Au-H octahedrons, and the corresponding vibration patterns are exhibited in Figs. 3(e) and 3(f). The accumulated $\lambda(\omega)$ suggests that the contribution of the low-frequency region below 30 meV mainly dominated by these two modes reaches ∼70% of total λ, which is significantly larger than that of the breathing mode of the Au-H octahedrons. These results suggest that searching the vibration mode with strong EPC would be an effective approach to discover high-T_c conventional superconductors.

To determine the superconducting T_c of Li_2AuH_6 under ambient pressure, we solve the anisotropic Eliashberg equations, and the superconducting gap Δ is shown in Fig. 4(a). The superconducting gap Δ is ∼26 meV at 55 K and eventually disappears at ∼140 K, which suggests that Li_2AuH_6

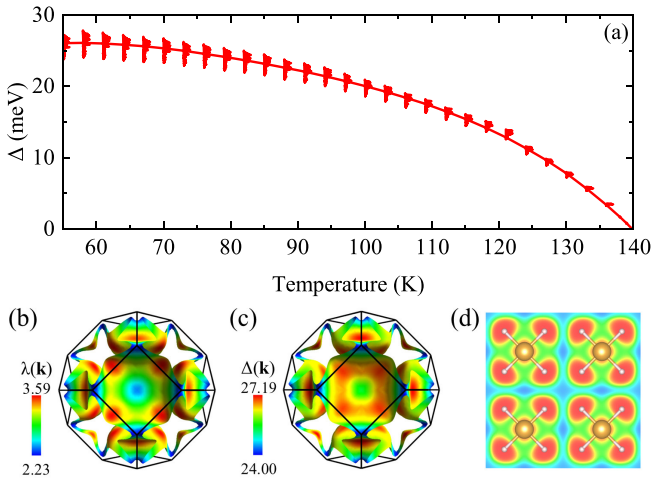

FIG. 4. (a) Normalized anisotropic superconducting gap Δ of Li_2AuH_6 under ambient pressure. The screening Coulomb potential μ^* is set to be 0.1. (b) Distribution of EPC $\lambda(\mathbf{k})$ on the Fermi surfaces. (c) Distribution of superconducting gap $\Delta(\mathbf{k})$ at 55 K on the Fermi surfaces. (d) Electron localization function of Li_2AuH_6. The yellow and pink atoms denote Au and H atoms, respectively.

possesses a high superconducting $T_c \sim 140$ K. Figures 4(b) and 4(c) show the anisotropic EPC and superconductivity of Li_2AuH_6. Relatively strong EPC electronic states exhibit a ring-like distribution upon the hemispherical Fermi surfaces. On the contrary, the electrons around the van Hove singularity contribute relatively weak EPC.

In Fig. 4(d), we show the electron localization function (ELF) of the crystal plane where the Au and H atoms lie. It is clearly seen that almost all valence electrons localize around H atoms. This kind of charge density is easily expected to change dramatically under those previously mentioned, strong EPC phonon modes. For example, the breathing mode of the Au-H octahedron and E_g mode at the X point where the Li and H atoms vibrate oppositely and become closer to each other [Figs. 3(d)–3(f)]. Generally, the metallic covalent bond is supposed to be beneficial to the stability of the crystal lattice and its metallization may induce strong EPC as well as high-T_c superconductivity. However, in this situation of Li_2AuH_6, there are no covalent bonds between the Au and H atoms while strong EPC and high T_c still exist. As an intuitive comparison, Pd and H possess quite close electronegativity, which suggests that electrons may exhibit more covalent properties than that in the Au-H system. However, the similar Li-Pd-H system [48] is not dynamically stable under ambient pressure and even shows a lower predicted superconducting T_c until a high pressure of 60 GPa than the ambient case of Li-Ag-H here. This may bring some helpful inspiration regarding the search of potential conventional superconductors in the future.

Discussion and Conclusion. The establishment of Bardeen-Cooper-Schrieffer (BCS) theory [49] provides a theoretical support for understanding and searching conventional superconductors. Metallizing the σ-bonding electrons [50,51] further proposes a possible way in finding high-T_c superconductors, which has also achieved success in explaining the superconductivity of MgB_2 [52]. Specifically, the σ-bonds formed by the in-plane B-$2p_{x/y}$ electrons strongly couple with an in-plane vibration mode of boron atoms [53]. Guided by this, many theoretical works are focusing on finding materials with metallic σ-bands. B possesses close electronegativity to H, hence the B-H system is regarded as a promising candidate. For example, KB_2H_8 is predicted to be a high-T_c BCS superconductor due to the strong EPC between the metallic B-H σ-electrons and the H-related phonon modes [23]. However, our studies here find the Au-H system without metallic σ-electrons can also exhibit high-T_c superconductivity, which leads us to realize that the strong coupling phonon that can cause a significant change of electronic density may be a more critical factor.

Hence, we propose a concept of the BCS superconducting unit, which provides strong EPC phonon modes as superconducting pairing glue, just like the superconducting unit of CuO planes provides antiferromagnetic fluctuation as glue for Cooper pairing in cuprates. Furthermore, the H octahedron with strong EPC phonon modes may be a potential BCS superconducting unit. One can try to design or synthesize more similar BCS superconducting units, such as the H tetrahedron, and so on, and stabilize them in the crystal lattice to find high-T_c BCS superconductors. In addition, considering the rising approaches of high-throughput calculations, crystal structure prediction, and artificial intelligence (AI), intercalating atoms directly in existing materials may introduce strongly coupled phonons into the system, which is a feasible way to investigate superconducting multicomponent compounds.

In this work, we first employed advanced AI technologies [32] to identify candidate materials with high T_c, and then conducted high-precision DFT calculations for the candidate materials recommended by AI. This approach differs from the traditional high-throughput DFT screening of materials. High-throughput methods, limited by the computational cost of DFT, can only perform coarse calculations for all materials, which frequently leads to misleading results due to insufficient computational accuracy. In contrast, AI-based searching can more precisely narrow down the range of target materials, thereby allowing more computational resources (such as introducing anisotropic corrections, refined electron-phonon coupling analysis, and other advanced computational strategies) to be allocated to more valuable candidate materials.

In summary, we use our developed AI search engine, namely, InvDesFlow [32], to identify a possible superconducting hydride Li_2AuH_6. Our studies of thermodynamics suggest a feasible route of experimental synthesis. By performing the first-principles density-functional theory and superconducting calculations, we find that Li_2AuH_6 exhibits a superconducting transition temperature of $\sim$140 K under ambient pressure. In addition to phonon modes of Au-H octahedrons that contribute strong EPC, the vibrations of Li atoms also play a crucial role. Furthermore, we propose that searching those superconducting units with strong EPC phonon modes may be an effective approach by combining them with methods of high-throughput calculations, crystal structure prediction, and artificial intelligence for finding high-T_c BCS superconductors.

Acknowledgments. This work was financially supported by the National Natural Science Foundation of China (Grants

No. 62476278, No. 12434009, and No. 12204533) and the Outstanding Innovative Talents Cultivation Funded Programs 2025 of Renmin University of China. Z.-Y.L. was also supported by the National Key R&D Program of China (Grants No. 2024YFA1408601). Computational resources were provided by the Physical Laboratory of High Performance Computing at Renmin University of China.

Data Availability. The data that support the findings of this article are openly available [35], embargo periods may apply.

[1] H. Kamerlingh Onnes, The resistance of pure mercury at helium temperatures, Comm. Phys. Lab. Univ. Leiden **12**, 120 (1911).

[2] N. W. Ashcroft, Metallic hydrogen: A high-temperature superconductor? Phys. Rev. Lett. **21**, 1748 (1968).

[3] Y. Li, J. Hao, H. Liu, Y. Li, and Y. Ma, The metallization and superconductivity of dense hydrogen sulfide, J. Chem. Phys. **140**, 174712 (2014).

[4] D. Duan, Y. Liu, F. Tian, D. Li, X. Huang, Z. Zhao, H. Yu, B. Liu, W. Tian, and T. Cui, Pressure-induced metallization of dense $(H_2S)_2H_2$ with high-T_c superconductivity, Sci. Rep. **4**, 6968 (2014).

[5] A. P. Drozdov, M. I. Eremets, I. A. Troyan, V. Ksenofontov, and S. I. Shylin, Conventional superconductivity at 203 kelvin at high pressures in the sulfur hydride system, Nature (London) **525**, 73 (2015).

[6] A. P. Drozdov, P. P. Kong, V. S. Minkov, S. P. Besedin, M. A. Kuzovnikov, S. Mozaffari, L. Balicas, F. F. Balakirev, D. E. Graf, V. B. Prakapenka, E. Greenberg, D. A. Knyazev, M. Tkacz, and M. I. Eremets, Superconductivity at 250 K in lanthanum hydride under high pressures, Nature (London) **569**, 528 (2019).

[7] M. Somayazulu, M. Ahart, A. K. Mishra, Z. M. Geballe, M. Baldini, Y. Meng, V. V. Struzhkin, and R. J. Hemley, Evidence for superconductivity above 260 K in lanthanum superhydride at megabar pressures, Phys. Rev. Lett. **122**, 027001 (2019).

[8] H. Liu, I. I. Naumov, R. Hoffmann, N. W. Ashcroft, and R. J. Hemley, Potential high-T_c superconducting lanthanum and yttrium hydrides at high pressure, Proc. Natl. Acad. Sci. USA **114**, 6990 (2017).

[9] F. Peng, Y. Sun, C. J. Pickard, R. J. Needs, Q. Wu, and Y. Ma, Hydrogen clathrate structures in rare earth hydrides at high pressures: Possible route to room-temperature superconductivity, Phys. Rev. Lett. **119**, 107001 (2017).

[10] H. Wang, J. S. Tse, K. Tanaka, T. Iitaka, and Y. Ma, Superconductive sodalite-like clathrate calcium hydride at high pressures, Proc. Natl. Acad. Sci. USA **109**, 6463 (2012).

[11] W. Chen, D. V. Semenok, X. Huang, H. Shu, X. Li, D. Duan, T. Cui, and A. R. Oganov, High-temperature superconducting phases in cerium superhydride with a T_c up to 115 K below a pressure of 1 megabar, Phys. Rev. Lett. **127**, 117001 (2021).

[12] D. V. Semenok, A. G. Kvashnin, A. G. Ivanova, V. Svitlyk, V. Y. Fominski, A. V. Sadakov, O. A. Sobolevskiy, V. M. Pudalov, I. A. Troyan, and A. R. Oganov, Superconductivity at 161 K in thorium hydride ThH_{10}: Synthesis and properties, Mater. Today **33**, 36 (2020).

[13] X. Li, X. Huang, D. Duan, C. J. Pickard, D. Zhou, H. Xie, Q. Zhuang, Y. Huang, Q. Zhou, B. Liu, and T. Cui, Polyhydride CeH_9 with an atomic-like hydrogen clathrate structure, Nat. Commun. **10**, 3461 (2019).

[14] N. P. Salke, M. M. D. Esfahani, Y. Zhang, I. A. Kruglov, J. Zhou, Y. Wang, E. Greenberg, V. B. Prakapenka, J. Liu, A. R. Oganov, and J.-F. Lin, Synthesis of clathrate cerium superhydride CeH_9 at 80-100 GPa with atomic hydrogen sublattice, Nat. Commun. **10**, 4453 (2019).

[15] D. Zhou, D. V. Semenok, D. Duan, H. Xie, W. Chen, X. Huang, X. Li, B. Liu, A. R. Oganov, and T. Cui, Superconducting praseodymium superhydrides, Sci. Adv. **6**, eaax6849 (2020).

[16] D. Zhou, D. V. Semenok, H. Xie, X. Huang, D. Duan, A. Aperis, P. M. Oppeneer, M. Galasso, A. I. Kartsev, A. G. Kvashnin, A. R. Oganov, and T. Cui, High-pressure synthesis of magnetic neodymium polyhydrides, J. Am. Chem. Soc. **142**, 2803 (2020).

[17] L. Ma, M. Zhou, Y. Wang, S. Kawaguchi, Y. Ohishi, F. Peng, H. Liu, G. Liu, H. Wang, and Y. Ma, Experimental clathrate superhydrides EuH_6 and EuH_9 at extreme pressure conditions, Phys. Rev. Res. **3**, 043107 (2021).

[18] Y.-L. Hai, H.-L. Tian, M.-J. Jiang, H.-B. Ding, Y.-J. Feng, G.-H. Zhong, C.-L. Yang, X.-J. Chen, and H.-Q. Lin, Prediction of high-T_c superconductivity in H_6SX (X = Cl, Br) at pressures below one megabar, Phys. Rev. B **105**, L180508 (2022).

[19] S. Di Cataldo, C. Heil, W. von der Linden, and L. Boeri, $LaBH_8$: Towards high-T_c low-pressure superconductivity in ternary superhydrides, Phys. Rev. B **104**, L020511 (2021).

[20] Z. Zhang, T. Cui, M. J. Hutcheon, A. M. Shipley, H. Song, M. Du, V. Z. Kresin, D. Duan, C. J. Pickard, and Y. Yao, Design principles for high-temperature superconductors with a hydrogen-based alloy backbone at moderate pressure, Phys. Rev. Lett. **128**, 047001 (2022).

[21] X. Liang, A. Bergara, X. Wei, X. Song, L. Wang, R. Sun, H. Liu, R. J. Hemley, L. Wang, G. Gao, and Y. Tian, Prediction of high-T_c superconductivity in ternary lanthanum borohydrides, Phys. Rev. B **104**, 134501 (2021).

[22] Y. Sun, J. Lv, Y. Xie, H. Liu, and Y. Ma, Route to a superconducting phase above room temperature in electron-doped hydride compounds under high pressure, Phys. Rev. Lett. **123**, 097001 (2019).

[23] M. Gao, X.-W. Yan, Z.-Y. Lu, and T. Xiang, Phonon-mediated high-temperature superconductivity in the ternary borohydride KB_2H_8 under pressure near 12 GPa, Phys. Rev. B **104**, L100504 (2021).

[24] M. Gao, P.-J. Guo, H.-C. Yang, X.-W. Yan, F. Ma, Z.-Y. Lu, T. Xiang, and H.-Q. Lin, Stabilizing a hydrogen-rich superconductor at 1 GPa by charge transfer modulated virtual high-pressure effect, Phys. Rev. B **107**, L180501 (2023).

[25] Y. Song, J. Bi, Y. Nakamoto, K. Shimizu, H. Liu, B. Zou, G. Liu, H. Wang, and Y. Ma, Stoichiometric ternary superhydride $LaBeH_8$ as a new template for high-temperature superconductivity at 110 K under 80 GPa, Phys. Rev. Lett. **130**, 266001 (2023).

[26] X. Song, X. Hao, X. Wei, X.-L. He, H. Liu, L. Ma, G. Liu, H. Wang, J. Niu, S. Wang, Y. Qi, Z. Liu, W. Hu, B. Xu, L.

Wang, G. Gao, and Y. Tian, Superconductivity above 105 K in nonclathrate ternary lanthanum borohydride below megabar pressure, J. Am. Chem. Soc. **146**, 13797 (2024).

[27] W. Chen, X. Huang, D. V. Semenok, S. Chen, D. Zhou, K. Zhang, A. R. Oganov, and T. Cui, Enhancement of superconducting properties in the LaCeH system at moderate pressures, Nat. Commun. **14**, 2660 (2023).

[28] K. Dolui, L. J. Conway, C. Heil, T. A. Strobel, R. P. Prasankumar, and C. J. Pickard, Feasible route to high-temperature ambient-pressure hydride superconductivity, Phys. Rev. Lett. **132**, 166001 (2024).

[29] A. Sanna, T. F. T. Cerqueira, Y.-W. Fang, I. Errea, A. Ludwig, and M. A. L. Marques, Prediction of ambient pressure conventional superconductivity above 80 k in hydride compounds, npj Comput. Mater. **10**, 44 (2024).

[30] F. Zheng, Z. Zhang, Z. Wu, S. Wu, Q. Lin, R. Wang, Y. Fang, C.-Z. Wang, V. Antropov, Y. Sun, and K.-M. Ho, Prediction of ambient pressure superconductivity in cubic ternary hydrides with MH_6 octahedra, Mater. Today Phys. **42**, 101374 (2024).

[31] X.-Q. Han, X.-D. Wang, M.-Y. Xu, Z. Feng, B.-W. Yao, P.-J. Guo, Z.-F. Gao, and Z.-Y. Lu, Ai-driven inverse design of materials: Past, present, and future, Chin. Phys. Lett. **42**, 027403 (2025).

[32] X.-Q. Han, Z. Ouyang, P.-J. Guo, H. Sun, Z.-F. Gao, and Z.-Y. Lu, InvDesFlow: An AI-driven materials inverse design workflow to explore possible high-temperature superconductors, Chin. Phys. Lett. **42**, 047301 (2025).

[33] Z.-F. Gao, S. Qu, B. Zeng, Y. Liu, J.-R. Wen, H. Sun, P.-J. Guo, and Z.-Y. Lu, AI-accelerated discovery of altermagnetic materials, Natl. Sci. Rev. nwaf066 (2025).

[34] See Supplemental Material at http://link.aps.org/supplemental/10.1103/PhysRevB.111.L140501 for the details of the AI search engine, and which includes Refs. [31,32].

[35] https://github.com/xqh19970407/InvDesFlow.

[36] P. Giannozzi, S. Baroni, N. Bonini, M. Calandra, R. Car, C. Cavazzoni, D. Ceresoli, G. L. Chiarotti, M. Cococcioni, I. Dabo, A. D. Corso, S. de Gironcoli, S. Fabris, G. Fratesi, R. Gebauer, U. Gerstmann, C. Gougoussis, A. Kokalj, M. Lazzeri, L. Martin-Samos *et al.*, QUANTUM ESPRESSO: A modular and open-source software project for quantum simulations of materials, J. Phys.: Condens. Matter **21**, 395502 (2009).

[37] J. P. Perdew, K. Burke, and M. Ernzerhof, Generalized gradient approximation made simple, Phys. Rev. Lett. **77**, 3865 (1996).

[38] D. R. Hamann, Optimized norm-conserving Vanderbilt pseudopotentials, Phys. Rev. B **88**, 085117 (2013).

[39] M. Methfessel and A. T. Paxton, High-precision sampling for Brillouin-zone integration in metals, Phys. Rev. B **40**, 3616 (1989).

[40] S. Baroni, S. de Gironcoli, A. Dal Corso, and P. Giannozzi, Phonons and related crystal properties from density-functional perturbation theory, Rev. Mod. Phys. **73**, 515 (2001).

[41] S. Poncé, E. Margine, C. Verdi, and F. Giustino, EPW: Electronphonon coupling, transport and superconducting properties using maximally localized Wannier functions, Comput. Phys. Commun. **209**, 116 (2016).

[42] G. Pizzi, V. Vitale, R. Arita, S. Blügel, F. Freimuth, G. Géranton, M. Gibertini, D. Gresch, C. Johnson, T. Koretsune, J. Ibañez-Azpiroz, H. Lee, J.-M. Lihm, D. Marchand, A. Marrazzo, Y. Mokrousov, J. I. Mustafa, Y. Nohara, Y. Nomura, L. Paulatto *et al.*, WANNIER90 as a community code: New features and applications, J. Phys.: Condens. Matter **32**, 165902 (2020).

[43] H. J. Choi, M. L. Cohen, and S. G. Louie, Anisotropic eliashberg theory of MgB_2: T_c, isotope effects, superconducting energy gaps, quasiparticles, and specific heat, Physica C: Superconductivity **385**, 66 (2003).

[44] E. R. Margine and F. Giustino, Anisotropic Migdal-Eliashberg theory using Wannier functions, Phys. Rev. B **87**, 024505 (2013).

[45] F. Giustino, Electron-phonon interactions from first principles, Rev. Mod. Phys. **89**, 015003 (2017).

[46] G. Yang, Y. Wang, F. Peng, A. Bergara, and Y. Ma, Gold as a 6p-element in dense lithium aurides, J. Am. Chem. Soc. **138**, 4046 (2016).

[47] W. Sun, S. T. Dacek, S. P. Ong, G. Hautier, A. Jain, W. D. Richards, A. C. Gamst, K. A. Persson, and G. Ceder, The thermodynamic scale of inorganic crystalline metastability, Sci. Adv. **2**, e1600225 (2016).

[48] X. L. Xia, Y. K. Wei, G. Xu, J. N. Yuan, J. M. Zhu, and D. Q. Wei, Chemically tuning stability and superconductivity of PdH compounds: A routine to high temperature superconductivity under modest pressures, J. Appl. Phys. **136**, 165901 (2024).

[49] J. Bardeen, L. N. Cooper, and J. R. Schrieffer, Microscopic theory of superconductivity, Phys. Rev. **106**, 162 (1957).

[50] M. Gao, Z.-Y. Lu, and T. Xiang, Prediction of phonon-mediated high-temperature superconductivity in $Li_3B_4C_2$, Phys. Rev. B **91**, 045132 (2015).

[51] M. Gao, Z.-Y. Lu, and T. Xiang, Finding high-temperature superconductors by metallizing the σ-bonding electrons, Physics **44**, 421 (2015).

[52] J. Nagamatsu, N. Nakagawa, T. Muranaka, Y. Zenitani, and J. Akimitsu, Superconductivity at 39 K in magnesium diboride, Nature (London) **410**, 63 (2001).

[53] K.-P. Bohnen, R. Heid, and B. Renker, Phonon dispersion and electron-phonon coupling in MgB_2 and AlB_2, Phys. Rev. Lett. **86**, 5771 (2001).